Front. Chem. Sci. Eng. 2019, 13(3): 574–585
https://doi.org/10.1007/s11705-019-1799-y

RESEARCH ARTICLE

Magnetic-porous microspheres with synergistic catalytic activity of small-sized gold nanoparticles and titania matrix

Kadriye Özlem Hamaloğlu[1], Ebru Sağ[2], Çiğdem Kip[1], Erhan Şenlik[1], Berna Saraçoğlu Kaya[2], Ali Tuncel (✉)[1]

1 Hacettepe University, Chemical Engineering Department, Ankara, Turkey
2 Cumhuriyet University, Chemical Engineering Department, Sivas, Turkey

Abstract Fe_3O_4 nanoparticles immobilized on porous titania in micron-size range were decorated with small-sized gold nanoparticles and used as a plasmonic catalyst for the reduction of 4-nitrophenol. Monodisperse-porous magnetic titania microspheres were synthesized with bimodal pore-size distribution by the sol-gel templating method. Small-sized gold nanoparticles obtained by the Martin method were attached onto the aminated form of the magnetic titania microspheres. A significant enhancement in the catalytic activity was observed using the gold nanoparticle-decorated magnetic titania microspheres compared to gold nanoparticle-decorated magnetic silica microspheres because of the synergistic effect between small-sized gold nanoparticles and titania. The synergistic effect for gold nanoparticle-attached magnetic titania microspheres could be explained by surface plasmon resonance-induced transfer of hot electrons from gold nanoparticles to the conduction band of titania. Using the proposed catalyst, 4-nitrophenol could be converted to 4-aminophenol in an aqueous solution within 0.5 min. The 4-nitrophenol reduction rates were 2.5–79.3 times higher than those obtained with similar plasmonic catalysts. The selection of micron-size, magnetic, and porous titania microspheres as a support material for the immobilization of small-sized gold nanoparticles provided a recoverable plasmonic catalyst with high reduction ability.

Keywords small-sized gold nanoparticles, magnetic titania microspheres, sol-gel template synthesis, plasmonic catalysis, 4-nitrophenol

1 Introduction

Literature surveys reveal that catalysts based on gold nanoparticles (AuNPs) can be used for many reactions, including the oxidation of carbon monoxide, alcohols, and diols, and the reduction of organic compounds [1−3]. Although AuNPs can perform their plasmonic catalytic activity without a solid support, their agglomeration in the reaction medium is a major disadvantage. To overcome this instability, different approaches, such as stabilization of AuNPs with polymers, dendrimers, and ligands [4], or their immobilization on porous solids like polymers, carbon-based materials, and metal oxides, have been attempted [4−10]. In addition to the colloidal stability, the immobilization of AuNPs on porous solids also allows easier removal of the catalyst from the reaction medium.

Titania-based nanocatalysts carrying AuNPs have been successfully used for reduction reactions [11−14]. Damato and co-workers described a facile approach for the immobilization of AuNPs on titania nanospheres and investigated the activity of the composite nanocatalyst as a function of its composition and particle size in the reduction of 4-nitrophenol (4-NP) [15]. Yazid et al. also prepared a catalyst for the reduction of 4-NP, in the form of AuNPs supported on titania, by the deposition-precipitation method [16]. The effect of AuNP size and pH on the catalytic activity were investigated [16]. Hyuntae et al. have synthesized a hybrid core–shell titanium glycolate-thiol-functionalized graphene composite for the immobilization of AuNPs [17].

In this study, the plasmonic catalytic activity of AuNP-decorated magnetic, monodisperse, and porous titania (AuNP@Mag-TiO_2) microspheres were prepared and utilized as a recoverable, efficient, synergistic catalyst for the reduction of 4-NP in batch fashion. The effects of AuNP size, AuNP loading, catalyst concentration, and 4-NP initial concentration on the catalytic activity were

Received July 27, 2018; accepted November 4, 2018

E-mail: atuncel@hacettepe.edu.tr

investigated using excess sodium borohydride ($NaBH_4$) in the reaction medium.

2 Experimental

2.1 Materials

The chemicals used in the synthesis of monodisperse-porous poly(3-chloro-2-hydroxypropyl methacrylate-*co*-ethylene glycol dimethacrylate) (poly(HPMA-Cl-*co*-EDMA) microspheres and poly(methacrylic acid-*co*-ethylene dimethacrylate) poly(MAA-*co*-EDMA) microspheres were purchased from Sigma-Aldrich Chemical Co., St. Louis, MO, USA, as reported earlier [18,19]. For the synthesis of polymethacrylate microspheres with amine groups starting from poly(HPMA-Cl-*co*-EDMA) microspheres, ethylene diamine (EDA, Sigma Chemical Co.) was used. Iron(II) chloride tetrahydrate ($FeCl_2 \cdot 4H_2O$), iron(III) chloride hexahydrate ($FeCl_3 \cdot 6H_2O$), and ammonium hydroxide solution (NH_4OH, 26% w/w) used for the magnetization of both amine-attached poly(HPMA-Cl-*co*-EDMA) and poly(MAA-*co*-EDMA) microspheres were purchased from Sigma-Aldrich Chemical Co. Titanium chloride, hexadecyltrimethylammonium bromide (CTAB), and tetrabutylammonium iodide (TBAI) were also purchased from Sigma-Aldrich Chemical Co. 3-Aminopropyltriethoxysilane (APTES) and triethylamine (TEA) used for the functionalization of magnetic titania microspheres were supplied from Sigma-Aldrich Chemical Co. For the synthesis of AuNPs, all chemicals were procured from Sigma-Aldrich Chemical Co. [20]. 4-Nitrophenol and $NaBH_4$ used in the catalytic activity runs were purchased from Aldrich Chem. Corp., WI, USA. Distilled deionized (DDI) water (Direct-Q 3 UV (Type 1), Millipore, USA) with a resistivity of 18 MΩ·cm was used in all runs.

2.2 Synthesis of magnetic titania (Mag-TiO_2) and magnetic silica (Mag-SiO_2) microspheres

Monodisperse, porous poly(HPMA-Cl-*co*-EDMA) microspheres and poly(MAA-*co*-EDMA) microspheres were utilized as the starting materials for the synthesis of magnetic titania (Mag-TiO_2) and magnetic silica (Mag-SiO_2) microspheres, respectively, and were synthesized by a multi-step microsuspension polymerization reaction [18,19,21,22].

The chemical route used for the synthesis of Mag-TiO_2 microspheres is given in Fig. 1(a). Typically, poly(HPMA-Cl-*co*-EDMA) microspheres (2.0 g) were treated with aqueous EDA solution (12.5 mL, 60% v/v) in a sealed reactor. The attachment of EDA onto poly(HPMA-Cl-*co*-EDMA) microspheres was performed in a shaking reactor at 80°C for 12 h. Subsequently, the EDA-attached poly (HPMA-Cl-*co*-EDMA) microspheres were washed with DDI water by centrifugation and decantation. The magnetization of EDA-attached poly(HPMA-Cl-*co*-EDMA) microspheres was performed according to the protocol described elsewhere [23]. Briefly, EDA-attached poly(HPMA-Cl-*co*-EDMA) microspheres (0.7 g) were dispersed in DDI water (100 mL) by ultrasonication for 1 min. The dispersion was stirred magnetically in an ice-bath for 15 min under a nitrogen blanket. $FeCl_3 \cdot 6H_2O$ (0.8 g) and $FeCl_2 \cdot 4H_2O$ (0.54 g) were dissolved in DDI water (20 mL) and this solution was added to the aqueous dispersion of EDA-attached poly(HPMA-Cl-*co*-EDMA) microspheres. The flask was evacuated under magnetic stirring after removing the ice-bath. The evacuation was continued until the dispersion stopped foaming and the flask was then immersed into an oil bath at 85°C. When the temperature of the solution reached 85°C, concentrated ammonia solution (25 mL, 25% w/w) was added to the dispersion, which immediately turned black. The resulting dispersion was stirred at 85°C for 1 h. After the dispersion was cooled to room temperature, the magnetic polymer microspheres were collected using a magnet and rinsed several times with water. The magnetic polymer microspheres were used as a template for the synthesis of monodisperse porous Mag-TiO_2 microspheres.

Mag-TiO_2 microspheres were synthesized by a staged-shape template hydrolysis and condensation protocol using magnetic, monodisperse poly(HPMA-Cl-*co*-EDMA) microspheres as the template material (Fig. 1(A)) [24]. For this purpose, the hydrous titanium dioxide ($TiO_2 \cdot nH_2O$) nanoparticles were obtained by hydrolysis of the selected precursor ($TiCl_4$) in an aqueous medium (60 mL, 0.1 $mol \cdot L^{-1}$). Next, the magnetic monodisperse poly(HPMA-Cl-*co*-EDMA) microspheres (0.4 g) were added into the precursor solution. The dispersion was stirred at 250 $r \cdot min^{-1}$ for 24 h at room temperature for the adsorption of $TiO_2 \cdot nH_2O$ nanoparticles onto the magnetic polymethacrylate microspheres. The microspheres were then collected by a magnet and washed extensively with DDI water. In the condensation step, the microspheres were dispersed in ammonia solution (60 mL, 1 $mol \cdot L^{-1}$) containing CTAB (0.3 g) as the stabilizer. The dispersion was stirred mechanically at 250 $r \cdot min^{-1}$ for 6 h at room temperature. The magnetic composite microspheres were again collected by a magnet and washed with DDI water to remove the excess chloride ions. These hydrolysis and condensation steps were performed twice. The magnetic composite microspheres were dried at 70°C for 12 h. Monodisperse porous Mag-TiO_2 microspheres were obtained after the calcination of the composite microspheres at 450°C for 4 h with a heating ramp of 2°C $\cdot min^{-1}$.

Mag-SiO_2 microspheres were also synthesized by a similar staged-shape template hydrolysis and condensation protocol using magnetic, monodisperse poly(MAA-*co*-EDMA) microspheres, as described in Fig. 1(b) [25]. In the first stage, poly(MAA-*co*-EDMA) microspheres were

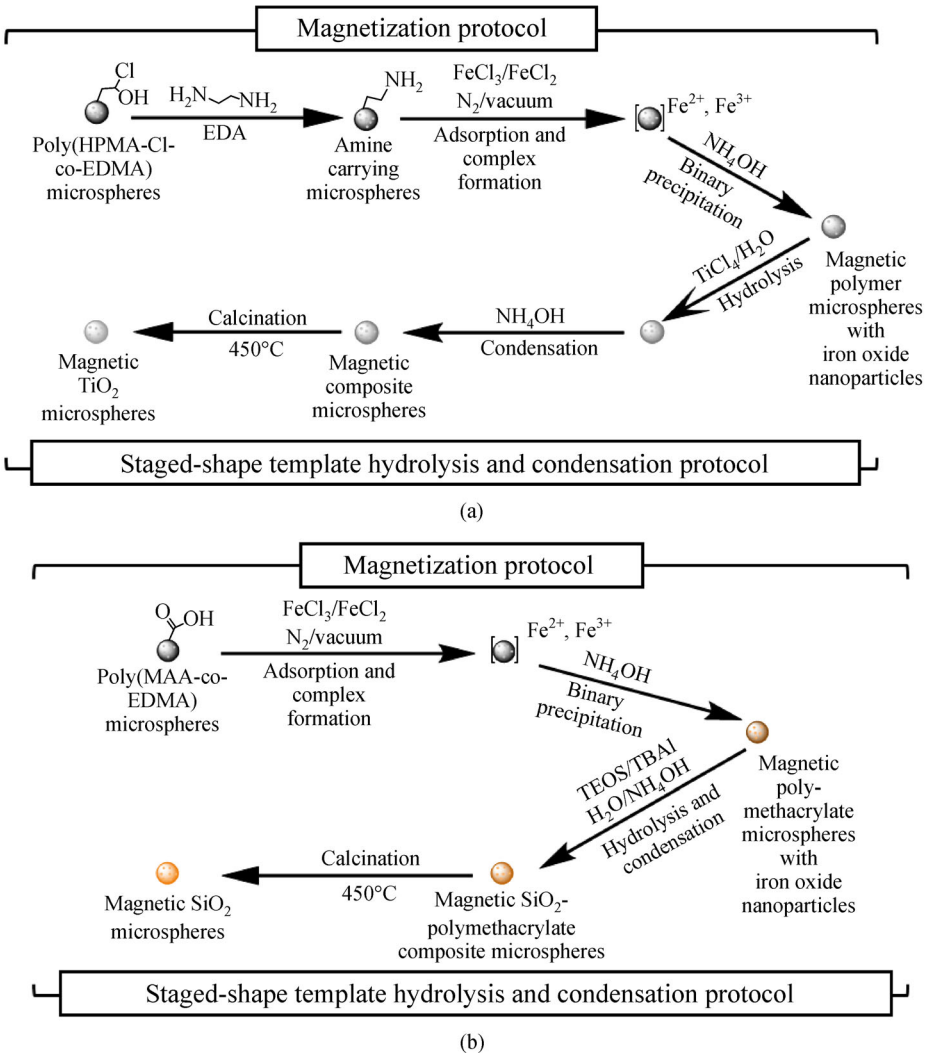

Fig. 1 Synthesis of monodisperse porous (a) Mag-TiO_2 and (b) Mag-SiO_2 microspheres by a staged-shape template hydrolysis and condensation protocol

magnetized by the binary precipitation of iron salts under the conditions used for the magnetization of EDA-attached poly(HPMA-Cl-*co*-EDMA) microspheres. For the synthesis of Mag-SiO_2 microspheres, the magnetic poly(MAA-*co*-EDMA) microspheres (0.4 g) were dispersed in a solution of 2-propanol (50 mL) and water (5 mL) containing TBAI (0.25 g), and concentrated ammonia (0.25 mL, 25% w/w). The silica precursor solution (5 mL) containing 25% v/v TEOS dissolved in 2-propanol was added dropwise. The dispersion was agitated at 350 r/min at room temperature for 24 h. The magnetic composite microspheres were collected using a magnet and washed with 2-propanol and DDI water. The washed microspheres were dried in vacuum at 60°C for 24 h. The calcination was performed at 450°C for 6 h with a heating ramp of 2°C·min^{-1} to obtain monodisperse-porous Mag-SiO_2 microspheres.

2.3 Synthesis of AuNP-attached magnetic titania (AuNP@Mag-TiO_2) and AuNP-attached magnetic silica (AuNP@Mag-SiO_2) microspheres

Prior to AuNP decoration, Mag-TiO_2 and Mag-SiO_2 microspheres were reacted with APTES in toluene [20]. In order to change the AuNP loading on Mag-TiO_2 microspheres, different amounts of amine-attached Mag-TiO_2 microspheres were put into AuNP solutions obtained via Turkevich and Martin methods (i.e., containing AuNPs 16 and 5 nm in size, respectively) and stirred mechanically at 300 r·min^{-1} for 6 h at room temperature [20]. Thus, Turkevich AuNP-decorated, magnetic, monodisperse, and porous titania (TAuNP@Mag-TiO_2) microspheres and Martin AuNP-decorated, magnetic, monodisperse, and porous titania (MAuNP@Mag-TiO_2) microspheres were obtained. After synthesis, both types of

microspheres were extensively washed with DDI water. The AuNP decoration protocol, identical to that applied for Mag-TiO_2 microspheres, was followed for obtaining the Martin AuNP-decorated, magnetic, monodisperse, and porous silica (MAuNP@Mag-SiO_2) microspheres. Thus, MAuNP@Mag-SiO_2 microspheres were obtained with the Au loading of 5% w/w [20].

2.4 Reduction of 4-NP with TAuNP@Mag-TiO_2 and MAuNP@Mag-TiO_2 microspheres

The catalytic activities of TAuNP@Mag-TiO_2 and MAuNP@Mag-TiO_2 microspheres were investigated in the reduction of 4-NP by changing the catalyst amount, initial 4-NP concentration, and Au loading on the Mag-TiO_2 microspheres. In a typical experiment, $NaBH_4$ (0.2 g) was added to an aqueous solution of 4-NP (7.5 $mg \cdot L^{-1}$, 26.5 mL) in a batch reactor. The solution was stirred with 300 $r \cdot min^{-1}$ at 20°C until evolution of H_2 gas had ceased. After a certain time, 500 μL of the sample was withdrawn from the reactor to determine the concentration of 4-NP. Next, TAuNP@Mag-TiO_2 or MAuNP@Mag-TiO_2 microspheres (1 mg) were added to the 4-NP solution. For the determination of 4-NP concentration in the aqueous medium at a certain time, the aforementioned microspheres were separated from the solution using an external magnet, and the sample (500 μL) was withdrawn from the liquid part not containing the magnetic catalyst microspheres. The concentration of 4-NP was determined by measuring the absorbance sample solution at 400 nm using a UV-Vis Spectrophotometer (UV-1601, Shimadzu, Japan). Reduction of 4-NP in batch fashion under the same conditions was also performed using MAuNP@Mag-SiO_2 microspheres as the catalyst instead of MAuNP@Mag-TiO_2 microspheres.

2.5 Catalyst recovery and reuse

The reusability of MAuNP@Mag-TiO_2 microspheres was investigated as it was selected as the best catalyst in the reduction of 4-NP. On the completion of catalytic reduction of 4-NP at 20°C with an initial 4-NP concentration of 7.5 $mg \cdot L^{-1}$, MAuNP@Mag-TiO_2 microspheres (1 mg) were separated using a magnet and rinsed with DDI water several times. The recovered catalyst was then reused for the degradation of 4-NP under the same conditions. This reduction-recovery cycle was repeated five times to test the reusability of the magnetic catalyst.

2.6 Characterization

The surface morphology and size distribution properties of all magnetic microspheres (i.e., Mag-TiO_2, MAuNP@-Mag-TiO_2, Mag-SiO_2, and MAuNP@Mag-SiO_2 microspheres) were determined by scanning electron microscopy (SEM; FEI- Quanta 200 FEG, USA). The surface chemical structures of all magnetic microspheres were investigated by energy dispersive X-ray spectroscopy (EDX). The magnetic behaviors of all magnetic microspheres were determined by the vibrating sample magnetometer (VSM, Quantum Design, Model P525, USA) at room temperature. For all magnetic microspheres, the pore size distributions and specific surface areas (SSAs) were determined by a surface area and pore size analyzer (Quantachrome, Nova 2200E, UK) using the Brunauer–Emmett–Teller equation. The crystal structures of all magnetic microspheres were determined by X-ray diffraction (XRD) spectroscopy (Rigaku, D/Max-2200, USA) and the chemical structures were investigated by Fourier transform infrared spectroscopy (Nicolet Nexus 470 FT-IR, Thermo Nicolet Co., USA).

3 Results and discussion

3.1 Characterization of plasmonic catalysts

The Mag-TiO_2 microspheres with size ~5.5 μm (coefficient of variation of 5.4%) and an SSA of 72.4 $m^2 \cdot g^{-1}$ were synthesized by following a staged-shape template hydrolysis and condensation protocol [24]. These microspheres exhibited a bimodal pore size distribution containing both mesoporous and macroporous compartments ranging between 3 and 145 nm in size. The median pore size in the mesoporous region was determined to be 16 nm and the macropores were ranged between 50 and 145 nm in size [24]. The saturation magnetization of Mag-TiO_2 microspheres was determined as 3.2 $emu \cdot g^{-1}$ [24]. No significant change was observed in the average size, SSA, and saturation magnetization by the deposition of Martin or Turkevich AuNPs onto Mag-TiO_2 microspheres.

The Mag-SiO_2 microspheres (6.0 μm in size with a coefficient of variation of 4.6% and an SSA of 235 $m^2 \cdot g^{-1}$) were synthesized by applying a similar staged-shape template hydrolysis and condensation protocol [25]. The saturation magnetization of Mag-SiO_2 microspheres was measured as 25.5 $emu \cdot g^{-1}$ [25]. No significant change was also observed in the average size, SSA, and saturation magnetization by the deposition of Martin AuNPs onto Mag-SiO_2 microspheres. The representative SEM photographs of MAuNP@Mag-TiO_2 and MAuNP@Mag-SiO_2 microspheres are given in Fig. 2. As seen here, both types of microspheres were obtained with a narrow size distribution. The shapes and surface morphologies of TAuNP@Mag-TiO_2 microspheres were also very similar to that observed for MAuNP@Mag-TiO_2 microspheres given in Fig. 2(a) [24]. The SEM photographs with higher magnification (i.e., 200000X) were also obtained for MAuNP@Mag-TiO_2 and MAuNP@Mag-SiO_2 microspheres and are presented in Figs. 2(a) and 2(b), respectively. These images revealed that MAuNPs were immobilized on the surfaces of both microspheres. On the

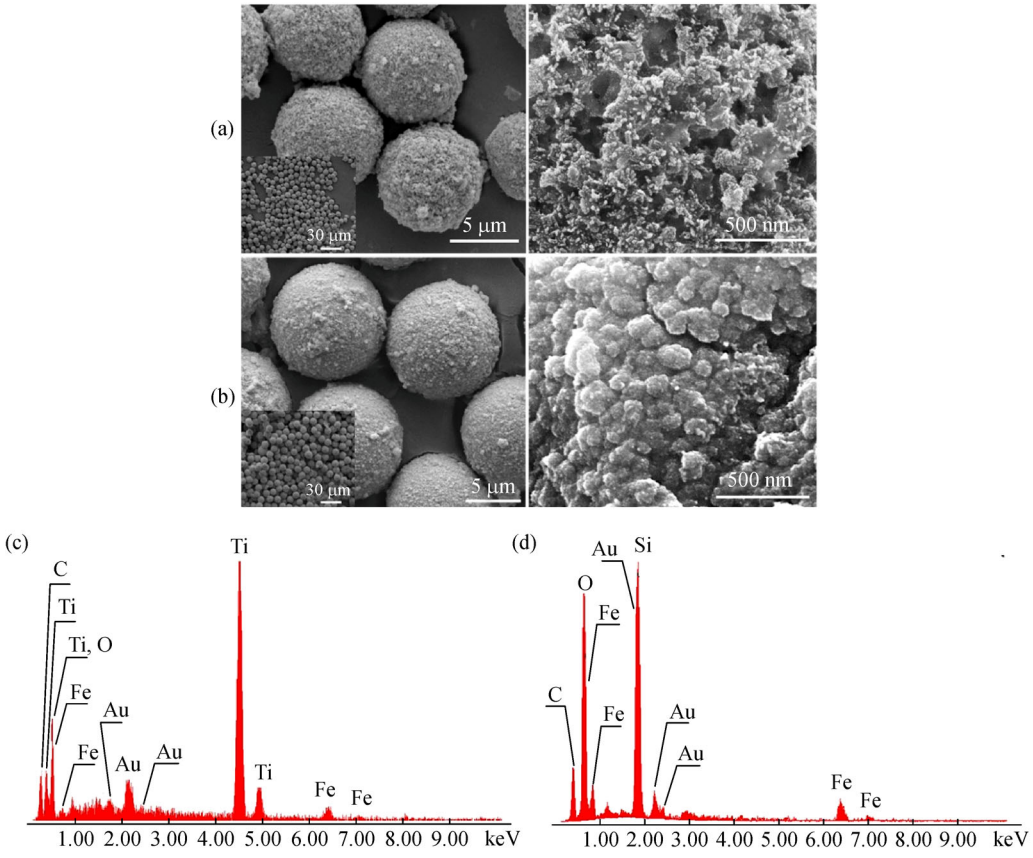

Fig. 2 (a) SEM photographs of MAuNP@Mag-TiO_2 microspheres, (b) SEM photographs of MAuNP@Mag-SiO_2 microspheres. Magnification: 20000X and 200000X, Magnification in the SEM photos showing size distribution: 2000X, (c) EDX spectrum of MAuNP@Mag-TiO_2 microspheres, (d) EDX spectrum of MAuNP@Mag-SiO_2 microspheres

other hand, the peaks belonging to Au, Fe, O, and Ti were obtained in the EDX spectrum of MAuNP@Mag-TiO_2 microspheres (Fig. 2(c)). As expected, the EDX spectrum of MAuNP@Mag-SiO_2 microspheres included Au, Fe, O, and Si (Fig. 2(d)). A weak peak corresponding to C was observed in both EDX spectra and likely originated from the carbonization of the polymethacrylate template during calcination, a step that was included in the synthesis of both MAu@Mag-TiO_2 and MAu@Mag-SiO_2 microspheres (Figs. 2(c) and 2(d)).

The presence of AuNPs and Fe_3O_4 NPs within MAuNP@Mag-TiO_2 and MAuNP@Mag-SiO_2 microspheres was shown by XRD (Fig. 3). For MAuNP@Mag-TiO_2 microspheres, the anatase peaks were obtained at 25.3°, 48.0°, 55.1°, 63.0°, 70.0° and 75°. The rutile peaks were observed at 27.4°, 36.1° and 40.5° [26−28]. In the XRD spectra of MAuNP@Mag-SiO_2 and MAuNP@Mag-TiO_2 microspheres, Fe_3O_4 peaks were found at 54° and 62° (i.e., marked by red lines) and the Au peaks were observed at 37.5°, 43.5° and 64° (i.e., marked by yellow dotted lines) [29,30]. The area ratios of Au and Fe_3O_4 peaks in the XRD spectrum of MAuNP@Mag-TiO_2 microspheres were not very different than those of MAuNP@Mag-SiO_2 microspheres. This finding may be evaluated as an evidence of MAuNP contents of Mag-SiO_2 and Mag-TiO_2 microspheres being close.

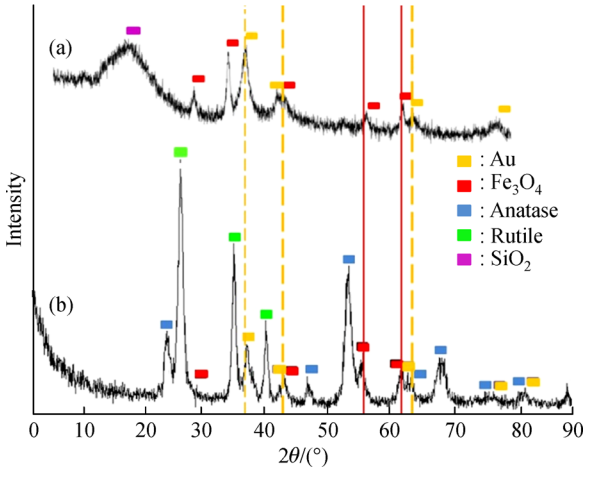

Fig. 3 XRD patterns of (a) MAuNP@Mag-SiO_2 and (b) MAuNP@Mag-TiO_2 microspheres

The FTIR spectra of Mag-TiO_2/MAuNP@Mag-TiO_2 and Mag-SiO_2/MAuNP@Mag-SiO_2 microspheres are given in Figs. S1(A) and S1(B), respectively. In all spectra,

the broad absorption bands lying between 3000 and 3700 cm^{-1} were assigned to the stretching vibrations of the O–H group of Mag-TiO_2/MAuNP@Mag-TiO_2 and Mag-SiO_2/MAuNP@Mag-SiO_2 microspheres [30−32]. For Mag-TiO_2 and MAuNP@Mag-TiO_2 microspheres, the spectra included absorption bands at 500 cm^{-1} and 1630 cm^{-1}, which were attributed to Ti–O–Ti stretching and Ti–O vibration in TiO_2, respectively (Fig. S1(A)) [30]. The intensive bands observed between 550 and 650 cm^{-1} in the FTIR spectra of Mag-TiO_2 and MAuNP@Mag-TiO_2 microspheres were assigned to the Fe–O bond vibration in Fe_3O_4 [30]. These broad bands observed for Mag-TiO_2 and MAuNP@Mag-TiO_2 microspheres could be ascribed to the overlapping of stretching vibrations originating from the Ti–O–Ti and Fe–O bonds at 590 cm^{-1}, which verified the magnetic titania structure [30]. In the FTIR spectra of Mag-SiO_2 and MAuNP@Mag-SiO_2 microspheres, the band at 570 cm^{-1} was attributed to the Si–O–Fe bond, which also verified the magnetic silica structure [32]. In the FTIR spectra of Mag-SiO_2 and MAuNP@Mag-SiO_2 microspheres, the broad absorption peaks located in the spectral range 1000−1100 cm^{-1} were assigned to the stretching vibrations of the Si–O bond. The absorption peaks at 960, 800, and 470 cm^{-1} were also in good agreement with the bending vibrations of the Si–O–Si bond [32].

The characterizations performed using SEM, EDX, FTIR, and XRD showed that the synthesized MAuNP@-Mag-TiO_2 and MAuNP@Mag-SiO_2 microspheres were monodisperse spherical particles including magnetic iron oxide in their structures and MAuNPs immobilized on their surfaces.

3.2 Reduction of 4-NP with plasmonic catalysts having synergistic activity

The schematic representation for the reduction of 4-NP to 4-aminophenol (4-AP) with AuNPs as a plasmonic catalyst using an excess amount of $NaBH_4$ is given in Fig. S2 [33]. As shown, 4-nitrophenolate ion was formed by the addition of $NaBH_4$ to the 4-NP solution. The absorption peak of 4-NP shifted from 313 to 400 nm after the addition of $NaBH_4$ because of the formation of 4-nitrophenolate ion, as evident from a color change from light yellow to dark yellow [34−36].

The reduction of 4-NP to 4-AP (the change in the intensity of absorption of nitrophenolate) was recorded by UV-Vis spectroscopy. The UV-Vis spectra recorded at different reaction periods during the reduction of 4-NP solution with TAuNP@Mag-TiO_2 microspheres using excess amount of $NaBH_4$ at 20°C are exemplified in Fig. 4. UV–Vis spectra shown in Fig. 4 indicated that the peak at 400 nm corresponded to the formation of 4-nitrophenolate anion on the addition of $NaBH_4$. Owing to the reduction of 4-NP with Turkevich AuNP-decorated magnetic titania microspheres, the intensity of 4-NP peak

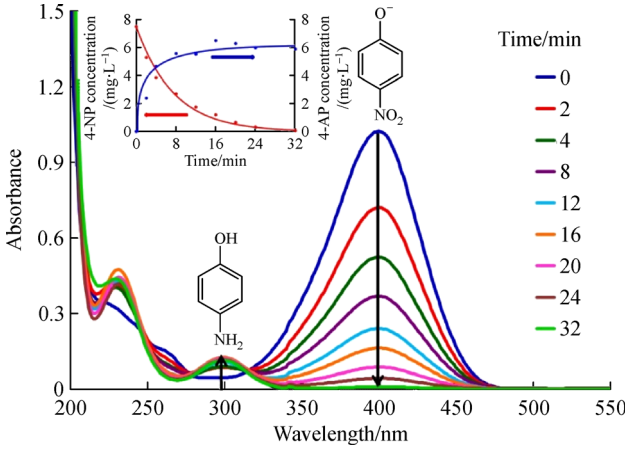

Fig. 4 UV-Vis spectra at different times during the plasmonic reduction of 4-NP with TAuNP@Mag-TiO_2 microspheres. Inset: Variation of 4-NP and 4-AP concentrations with the time. Calcination temperature: 450°C, AuNP loading: 5% w/w; catalyst amount: 1 mg, 4-NP concentration: 7.5 $mg \cdot L^{-1}$, 26.5 mL, temperature: 20°C

at 400 nm decreased continuously, while the intensity of 4-AP peak at 300 nm increased. The concentration of 4-NP was calculated according to the decrease in the absorbance peak at 400 nm, which was directly proportional to the reduction in 4-NP concentration. The variation of 4-NP and 4-AP concentrations with time during the reduction of 4-NP solution containing TAuNP@Mag-TiO_2 microspheres is given as an inset in Fig. 4. As seen here, 4-NP was completely converted to 4-AP within 32 min under the studied conditions.

In the literature, various AuNP@TiO_2 nanocomposites have been prepared as plasmonic or photocatalytic materials, particularly using conventional TiO_2 nanoparticles [11−17]. The isolation and recovery of the catalyst is usually difficult when it is utilized in the form of nanoparticles in batch fashion. In the present study, the monodisperse porous Mag-TiO_2 microspheres of size 5.5 μm were selected as a support material for the synthesis of the plasmonic catalyst. Both the magnetic property and the particle size in the micron range allowed an easier and fast isolation of the plasmonic catalyst as compared to the nanoparticle-based catalytic materials. The optical images of the color changes observed in the conversion of 4-NP to 4-AP are given in Fig. S3. As shown, a clear solution with almost zero absorbance in the visible region (i.e., at a wavelength of 500 nm) was obtained within a time-period of less than 1 min, by the separation (or collection) of MAuNP@Mag-TiO_2 microspheres by an external magnet.

The effect of AuNP size on the reduction rate of 4-NP was investigated by using TAuNP@Mag-TiO_2, MAuNP@Mag-TiO_2, and MAuNP@Mag-SiO_2 microspheres as plasmonic catalysts. In these runs, TiO_2, Mag-TiO_2, and Mag-SiO_2 microspheres were also included as

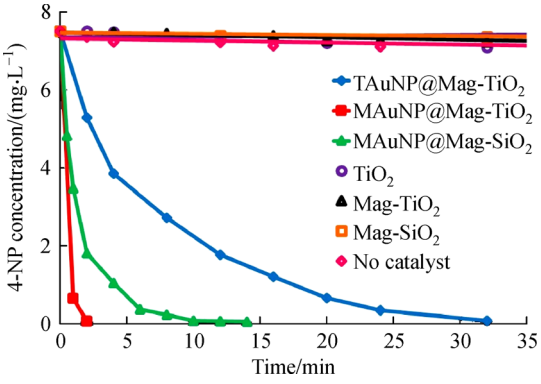

Fig. 5 Variation of 4-NP concentration with time using TAuNP@Mag-TiO_2, MAuNP@Mag-TiO_2, and MAuNP@Mag-SiO_2 microspheres as plasmonic catalysts and reference materials (i.e., TiO_2, Mag-TiO_2, and Mag-SiO_2). Calcination temperature: 450°C; AuNP loading: 5% w/w; catalyst amount: 1 mg; 4-NP concentration: 7.5 mg·L^{-1}, 26.5 mL; temperature: 20°C

references for comparison (Fig. 5).

As shown, the decrease in 4-NP concentration was only due to the reduction of 4-NP with AuNP-decorated magnetic microspheres and not because of the adsorption of 4-NP onto the bare and magnetic microspheres. The MAuNP@Mag-TiO_2 and TAuNP@Mag-TiO_2 microspheres used in this study were prepared using AuNPs that were 5 and 16 nm in size, respectively [20]. As seen in Fig. 5, a significant enhancement in the reduction of 4-NP was observed by using MAuNP@Mag-TiO_2 microspheres, in which the AuNP size was smaller, as compared to TAuNP@Mag-TiO_2 microspheres. The time needed for the complete reduction of 4-NP solution decreased from 32 min to 2 min because of the higher redox potential of small-sized AuNPs supported on Mag-TiO_2 microspheres. It has been reported that AuNPs of smaller size have a higher redox potential, which accelerates the electron transfer and thereby increases the reaction rate of catalytic reactions [35]. As seen in Fig. 5, a higher catalytic activity was achieved with the MAuNP@Mag-TiO_2 microspheres as compared to MAuNP@Mag-SiO_2 microspheres that were synthesized following a very similar protocol and with very similar sizes and porous properties (Figs. 1 and 2). This difference in plasmonic activity can probably be explained by the efficient electron transfer between AuNPs and TiO_2 or a higher amount of Martin AuNP deposited onto Mag-TiO_2 in comparison to Mag-SiO_2. However, the deposition of a higher amount of MAuNP onto Mag-TiO_2 as compared to Mag-SiO_2 was not supported by the XRD data (Fig. 3). Therefore, the higher plasmonic activity of AuNP@Mag-TiO_2 microspheres could only be explained by the efficient electron transfer taking place between AuNPs and TiO_2. As expected, no significant 4-NP conversion was observed in the presence of selected reference materials (i.e., TiO_2, Mag-TiO_2, and Mag-SiO_2 microspheres) because no AuNPs were present on them. The kinetic results in Fig. 5 clearly show that the highest 4-NP consumption rate was achieved with the MAuNP@Mag-TiO_2 microspheres.

The effect of initial 4-NP concentration on the reduction rate of 4-NP with TAuNP@Mag-TiO_2 and MAuNP@Mag-TiO_2 microspheres is given in Fig. 6. As seen in Fig. 6(a), the reduction rate of 4-NP markedly decreased with the increasing initial concentration of 4-NP in the presence of TAuNP@Mag-TiO_2 microspheres. This decrease was likely attributable to the inadequate amount of AuNPs for the reduction of more 4-NP molecules. As the reduction rate of 4-NP increased dramatically on reducing the size of AuNPs decorating the Mag-TiO_2 microspheres, a complete reduction of 4-NP with the highest concentration (15 mg·L^{-1}) was achieved within 2 min by using MAuNP@Mag-TiO_2 microspheres as the plasmonic catalysts (Fig. 6(b)). As shown in this figure, although the initial concentration was increased two-fold (from 7.5 to 15 mg·L^{-1}), an almost complete reduction of 4-NP was achieved within the same period (2 min). This

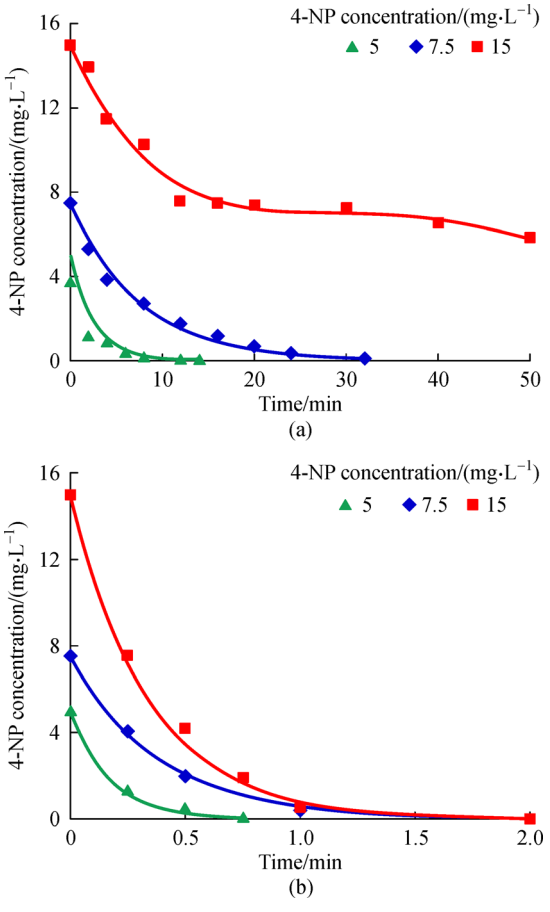

Fig. 6 Effect of the initial 4-NP concentration on the plasmonic reduction rate of 4-NP with (a) TAuNP@Mag-TiO_2 and (b) MAuNP@Mag-TiO_2 microspheres. Calcination temperature: 450°C; AuNP loading: 5% w/w; catalyst amount: 1 mg; temperature: 20°C

behavior can be assessed as a clear evidence of the enhancement of plasmonic catalytic activity of AuNP@-Mag-TiO_2 microspheres on reducing the AuNP size. Recently, magnetic Fe_3O_4@CeO_2 nanoparticles (~300 nm) loaded with Pt or Pd nanoparticles were proposed as a superior plasmonic catalyst for 4-NP reduction in batch fashion [37]. In the cited study, 4-NP (10 $mg \cdot L^{-1}$) was completely converted to 4-AP in the presence of excess $NaBH_4$ by using a catalyst concentration of 0.05 $mg \cdot mL^{-1}$ in a reaction volume of 40 mL, with the reaction times ranging between 3 and 7 min depending upon the noble metal nanoparticles (Pt, Pd, or Pt-Pd) incorporated into the magnetic Fe_3O_4@CeO_2 nanocomposite [37]. In the present case, 15 $mg \cdot L^{-1}$ of 4-NP could be completely converted to 4-AP in the reaction volume of 26.5 mL within 2 min using a plasmonic catalyst (i.e., MAuNP@Mag-TiO_2) concentration of 0.038 $mg \cdot mL^{-1}$. The average 4-NP reduction rate obtained with MAuNP@Mag-TiO_2 microspheres was 0.795 $\mu mol_{4\text{-NP}} \cdot mg_{catalyst}^{-1} \cdot min^{-1}$ for the complete reduction of 4-NP.

The concentration-time curves given in Fig. 6 were evaluated by considering the pseudo-first order kinetics for the plasmonic reduction of 4-NP, as also performed previously [5,15,16]. For this purpose, $\ln(C_{4\text{-NP}}/C_{4\text{-NP}}^{o})$ was plotted against time for different 4-NP initial concentrations ($C_{4\text{-NP}}$ and $C_{4\text{-NP}}^{o}$ are the concentration of 4-NP at any time and the initial concentration, respectively). The straight lines used for the determination of the first order apparent rate constants are given in Figs. S4(A) and S4(B) for TAuNP@Mag-TiO_2 and MAuNP@Mag-TiO_2 microspheres as plasmonic catalysts, respectively. The determined values of apparent rate constants for different 4-NP initial concentrations are presented in Table 1.

The apparent rate constant decreased with the increasing 4-NP initial concentration for both TAuNP@Mag-TiO_2 and MAuNP@Mag-TiO_2 microspheres (Table 1). As expected, the rate constants calculated for the MAuNP@-Mag-TiO_2 microspheres were higher as compared to those for the TAuNP@Mag-TiO_2 microspheres. The first order apparent rate constants varying between 1.0 and 2.3 $min^{-1} \cdot mg_{catalyst}^{-1}$ were reported for AuNP carrying monodisperse colloidal TiO_2 nanoparticles with an initial 4-NP concentration of 1.36 $mg \cdot L^{-1}$ [15]. In the present case, the apparent rate constant calculated with the lowest 4-NP initial concentration with the MAuNP@Mag-TiO_2 microspheres (i.e., 5.852 $min^{-1} \cdot mg_{catalyst}^{-1}$ for 4-NP initial concentration of 5.0 $mg \cdot L^{-1}$) was considerably higher as compared to the reported values of AuNP carrying monodisperse-colloidal TiO_2 nanoparticles [15].

The effect of AuNP loading on the catalytic reduction rate of 4-NP is given in Fig. 7. As shown, the complete reduction of 4-NP was achieved within 2 min for all AuNP loadings. An apparent effect of AuNP loading on the catalytic activity of MAuNP@Mag-TiO_2 microspheres was not observed in the studied range.

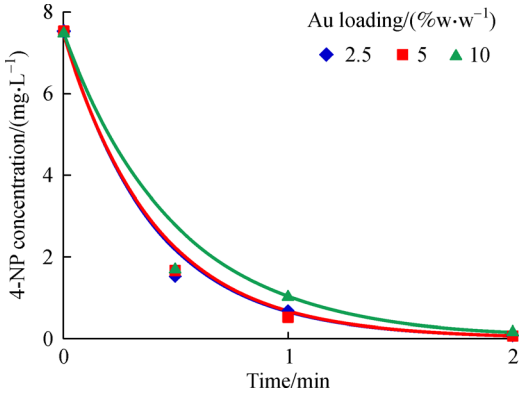

Fig. 7 Effect of AuNP loading on the reduction rate of 4-NP with MAuNP@Mag-TiO_2 microspheres. Calcination temperature: 450°C; catalyst amount: 1 mg; 4-NP concentration: 7.5 $mg \cdot L^{-1}$, 26.5 mL; Temperature: 20°C

The effect of the catalyst amount on the plasmonic reduction rate of 4-NP by using MAuNP@Mag-TiO_2 microspheres is illustrated in Fig. 8. As expected, the reduction rate of 4-NP increased on increasing the amount of MAuNP@Mag-TiO_2 microspheres [34−36]. The complete reduction of 4-NP was achieved in less than 20 s with the highest amount of the catalyst (i.e., 4 mg in 26.5 mL of reaction volume). For this run, the average 4-NP consumption rate was calculated as 1.19 $\mu mol_{4\text{-NP}} \cdot mg_{catalyst}^{-1} \cdot min^{-1}$. The highest 4-NP reduction rate for

Table 1 First-order apparent rate constants for 4-NP reduction by AuNP@Mag-TiO_2 microspheres as plasmonic catalyst for different initial concentrations of 4-NP [a)]

Catalyst type	4-NP Initial concentration /($mg \cdot L^{-1}$)	k_{app} /($min^{-1} \cdot mg_{catalyst}^{-1}$)
TAuNP@Mag-TiO_2 microspheres	5.0	0.353
	7.5	0.133
	15.0	0.024
MAuNP@Mag-TiO_2 microspheres	5.0	5.852
	7.5	2.589
	15.0	2.927

a) catalyst concentration: 0.038 $mg \cdot mL^{-1}$, reaction volume: 26.5 mL, 20°C

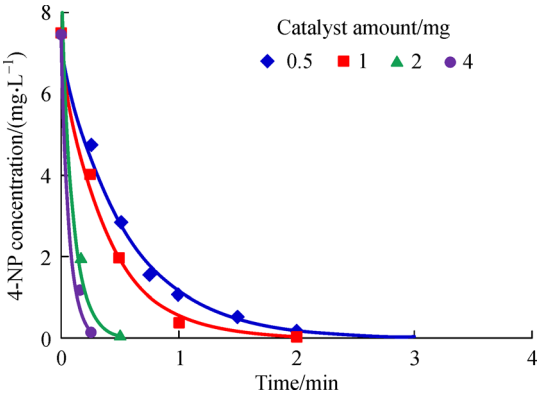

Fig. 8 Effect of catalyst amount on the plasmonic reduction rate of 4-NP with MAuNP@Mag-TiO_2 microspheres. Calcination temperature: 450°C, AuNP loading: 5% w/w; 4-NP concentration: 7.5 mg·L^{-1}, 26.5 mL, temperature: 20°C

Pd-loaded magnetic Fe_3O_4@CeO_2 nanoparticles was calculated as 0.50 $\mu mol_{4\text{-NP}} \cdot mg_{catalyst}^{-1} \cdot min^{-1}$ on considering the complete conversion of 4-NP within 3 min, according to the reported data [37]. In another study, poly (allylamine hydrochloride)-modified polymer poly(glycidyl methacrylate) composite sub-microspheres with tunable gold nanoparticles (PGMA@PAH@AuNPs) were evaluated as plasmonic catalysts for 4-NP reduction [5]. The 4-NP reduction rate was calculated as 0.393 $\mu mol_{4\text{-NP}} \cdot mg_{catalyst}^{-1} \cdot min^{-1}$ by using the data for complete conversion of 4-NP within 2.13 min [5]. AuNP-attached colloidal TiO_2 nanoparticles (~220 nm in diameter) were also used as plasmonic catalysts for 4-NP reduction in batch fashion [15]. For the referred study, the highest average 4-NP reduction rate was calculated as 0.015 $\mu mol_{4\text{-NP}} \cdot mg_{catalyst}^{-1} \cdot min^{-1}$ by considering 90% (w/w) of 4-NP conversion within 30 min, by using the reported data for the catalyst encoded as TiO_2–Au [15]. In this study, the 4-NP reduction rates obtained with MAuNP@Mag-TiO_2 microspheres were 2.4−79.3 times higher as compared to similar plasmonic catalysts. Hence, the plasmonic catalytic performance of MAuNP@Mag-TiO_2 microspheres was superior with respect to the plasmonic catalysts, particularly those containing Au and TiO_2 nanoparticles. The deposition of a higher amount of small-sized AuNPs onto a relatively larger surface area of magnetic-porous TiO_2 microspheres originating from their bimodal pore size distribution containing both mesoporous and macroporous compartments was likely the reason for the higher 4-NP reduction rate observed with the MAuNP@Mag-TiO_2 catalyst. The concentration-time curves in Fig. 8 were evaluated according to pseudo-first order kinetics for plasmonic reduction of 4-NP by MAuNP@Mag-TiO_2 microspheres. The curves used for the calculation of the first order apparent rate constants for different MAuNP@-Mag-TiO_2 concentrations are given in Fig. S5.

The determined values of apparent rate constants (min^{-1}) are given in Table 2. As seen here, the apparent rate constants were also expressed in term of $min^{-1} \cdot mg_{catalyst}^{-1}$ by dividing the determined value by the amount of catalyst used. As expected, the rate constants given as min^{-1} increased with increasing catalyst concentration. However, when these values were divided by the amount of catalyst used, the apparent rate constants varied between 2.6 and 4.8 per mg of the catalyst in each run (i.e., $min^{-1} \cdot mg_{catalyst}^{-1}$) (Table 2). An average value of these individual runs (3.659 $min^{-1} \cdot mg_{catalyst}^{-1}$) was also considerably higher with respect to the apparent rate constants reported for AuNP carrying monodisperse colloidal TiO_2 nanoparticles [15].

Table 2 First-order apparent rate constants for 4-NP reduction for different MAuNP@Mag-TiO_2 concentrations[a)]

MAuNP@Mag-TiO_2 concentration /(mg·mL^{-1})	k_{app} /min^{-1}	k_{app} /($min^{-1} \cdot mg_{catalyst}^{-1}$)
0.019 (0.5)[b)]	1.834	3.668
0.038 (1.0)[b)]	2.589	2.589
0.076 (2.0)[b)]	9.492	4.746
0.152 (4.0)[b)]	14.532	3.633

a) 4-NP initial concentration: 7.5 mg·L^{-1}; Reaction volume: 26.5 mL, 20°C; b) amount of catalyst/mg used in the reaction volume of 26.5 mL is given within the parenthesis

3.3 Mechanism of synergistic catalytic activity

In a recent study, a nanocatalyst that is very similar to the one synthesized in this work has been developed and the term “synergistic catalytic activity” has been used for the first time for 4-NP reduction [38]. The reported synergistic nanocatalyst was produced in the form of AuNP-loaded hierarchical hollow porous TiO_2 nanospheres, ~355 nm in size, and evaluated for the reduction of 4-NP under visible or UV-light irradiation [38]. In the referred study, the synergistic catalytic activity of the AuNP-loaded hollow porous TiO_2 nanospheres under visible light was explained by the injection of hot electrons, generated by surface plasmon resonance (SPR) of AuNPs, to the conduction band of hollow TiO_2 nanoparticles as the energy of hot electrons relative to the Au Fermi level was higher than the Schottky barrier height [39−43]. This electron transfer was termed as the “nanojet effect” of hollow and porous TiO_2 nanospheres [38]. The hot electrons were transferred through the hollow, porous TiO_2 nanospheres to the lowest unoccupied molecular orbital (LUMO) of 4-NP. The reduced surface electron density of AuNPs, owing to the hot electron transfer from AuNPs to the hollow, porous TiO_2 nanospheres enhanced both the adsorption of BH_4^- and 4-NP onto AuNPs and the electron transfer from BH_4^- to 4-NP through the AuNPs [38]. Hence, 4-NP reduction rate increased. Although the reduction conditions were somewhat different, the comparison of the reaction periods for complete reduction of 4-NP showed that the reduction

rates obtained in our study were roughly in the same order of magnitude as those obtained with AuNP-loaded hierarchical hollow and porous TiO_2 nanospheres [38]. In the present case, a plasmonic catalyst with a very similar structure was obtained by the immobilization of Martin Au nanoparticles (MAuNPs) onto porous TiO_2 microspheres in the magnetic form. Considering the "synergistic catalytic activity" concept proposed for 4-NP reduction by AuNP loaded-hollow porous TiO_2 nanospheres, the possible reaction mechanisms for 4-NP reduction with MAuNP@Mag-SiO_2 and MAuNP@Mag-TiO_2 microspheres can be explained as given in Fig. 9. In the case of catalytic reduction of 4-NP by MAuNP@Mag-SiO_2 microspheres, SPR-induced electrons are transferred from BH_4^- ions as a nucleophile to MAuNPs and then to 4-NP adsorbed onto Mag-SiO_2 microspheres, as an electrophile that captures electrons from MAuNPs [44–46]. Thus, the reduction of 4-NP with $NaBH_4$ in the presence of MAuNP@Mag-SiO_2 microspheres only proceeds with MAuNPs as a noble metal catalyst [44–46]. In the case of catalytic reduction of 4-NP by MAuNP@Mag-TiO_2 microspheres, the catalytic reduction involves both MAuNPs and MagTiO_2 microspheres [38]. The SPR-induced hot electrons generated by MAuNPs are transferred to the conduction band of magnetic-porous TiO_2 microspheres [38]. Hence, these hot electrons are transported from the porous TiO_2 microspheres to the LUMO of 4-NP [38,47]. The reaction was facilitated because of electron transfer from MAuNPs to TiO_2, which reduced the electron density of MAuNPs and promoted the adsorption of both BH_4^- and 4-NP onto MAuNPs [38,44–46]. It could be deduced that the synergistic catalytic effect between MAuNPs and TiO_2 was due to the transfer of hot electrons from MAuNPs to the conduction band of TiO_2, which apparently enhanced the rate of reduction of 4-NP.

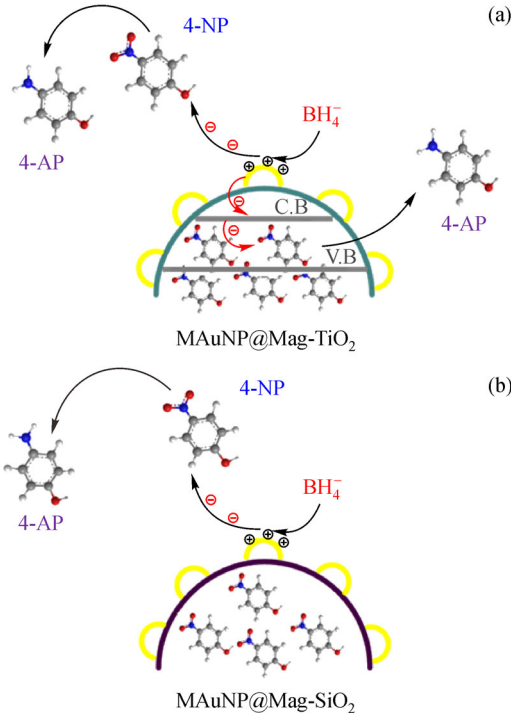

Fig. 9 Possible mechanisms for 4-NP reduction with (a) MAuNP@Mag-TiO_2 and (b) MAuNP@Mag-SiO_2 microspheres

3.4 Reusability of plasmonic catalyst

To assess the reusability MAuNP@Mag-TiO_2 microspheres having the highest catalytic activity, the reduction of 4-NP at 20°C was repeated five times under the same conditions (Fig. 10). After each run, the plasmonic catalyst was recovered using an external magnet. The percentage of removal in each cycle is given in Fig. 10. The percentage removal of 4-NP decreased by 1.7% after three cycles and it was 89.9% after being reused five times. This decrease could be ascribed to the adsorption of 4-AP, which was formed during plasmonic degradation onto MAuNP@-Mag-TiO_2 microspheres.

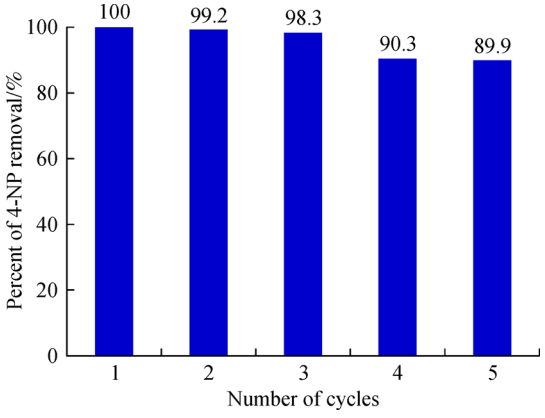

Fig. 10 Reusability of MAuNP@Mag-TiO_2 microspheres for plasmonic reduction of 4-NP. Calcination temperature: 450°C; AuNP loading: 5% w/w; catalyst amount: 1 mg; 4-NP concentration: 7.5 mg·L^{-1}, 26.5 mL; temperature: 20°C

4 Conclusions

The catalytic activity of AuNP@Mag-TiO_2 microspheres was investigated in the reduction of 4-NP by changing the AuNPs size, AuNP loading, catalyst amount, and initial concentration of 4-NP. A significant enhancement in the plasmonic catalytic activity was observed with MAuNP@-Mag-TiO_2 microspheres, in which the AuNP size was smaller in comparison to the TAuNP@Mag-TiO_2 microspheres. The MAuNP@Mag-TiO_2 microspheres also exhibited a higher catalytic activity with respect to MAuNP@Mag-SiO_2 microspheres synthesized following a similar protocol and with a very similar size and porous properties. This difference could probably be explained by an efficient electron transfer between TiO_2 and AuNPs. The synergistic catalytic effect of AuNP@Mag-TiO_2

microspheres could be explained by surface plasmon resonance-induced transfer of hot electrons from AuNPs to the conduction band of titania (i.e., nanojet effect) [38]. The selection of magnetic porous TiO_2 particles in micron-size range as a component of the proposed system provided an easily recoverable plasmonic catalyst with superior activity with respect to the previously synthesized similar catalysts [5,15,37]. The complete reduction of 4-NP was achieved within 0.5 min in the catalytic runs performed using MAuNP@Mag-TiO_2 microspheres.

Acknowledgements Special thanks are extended to the Turkish Academy of Sciences (TUBA) for research support provided to Prof. Ali Tuncel as a full member.

Electronic Supplementary Material Supplementary material is available in the online version of this article at https://doi.org/10.1007/s11705-019-1799-y and is accessible for authorized users.

References

1. Hutchings G J, Haruta M. A golden age of catalysis: A perspective. Applied Catalysis A, General, 2005, 291(1-2): 2–5
2. Haruta M. Catalysis: Gold rush. Nature, 2005, 437(1): 1098–1099
3. Wittstock A, Zielasek V, Biener J, Friend C M, Bäumer M. Nanoporous gold catalysts for selective gas-phase oxidative coupling of methanol at low temperature. Science, 2010, 327 (5963): 319–322
4. Didier A, Feng L, Jaime R A. Nanoparticles as recyclable catalysts: The frontier between homogeneous and heterogeneous catalysis. Angewandte Chemie International Edition, 2005, 44(1): 7852–7872
5. Maolin L, Guofang C. Revisiting catalytic model reaction *p*-nitrophenol/$NaBH_4$ using metallic nanoparticles coated on polymeric spheres. Nanoscale, 2013, 5(23): 11919–11927
6. Kyoko K, Tamao I, Masatake H. Reduction of 4-nitrophenol to 4-aminophenol over Au nanoparticles deposited on PMMA. Journal of Molecular Catalysis A Chemical, 2009, 298(1-2): 7–11
7. Wang D, Villa A, Su D, Prati L, Schlögl R. Carbon-supported gold nanocatalysts: Shape effect in the selective glycerol oxidation. ChemCatChem, 2013, 5(9): 2717–2723
8. Wang C, Chen L, Qi Z. One-pot synthesis of gold nanoparticles embedded in silica for cyclohexane oxidation. Catalysis Science & Technology, 2013, 3(4): 1123–1128
9. Donoeva B G, Ovoshchnikov D S, Golovko V B. Establishing Au nanoparticle size effect in the oxidation of cyclohexene using gradually changing Au catalysts. ACS Catalysis, 2013, 3(12): 2986–2991
10. Wang Y, Van de Vyver S, Sharma K, Román-Leshkov Y. Insights into the stability of gold nanoparticles supported on metal oxides for the base-free oxidation of glucose to gluconic acid. Green Chemistry, 2014, 16(2): 719–726
11. Cardenas-Lizana F, Gomez-Quero S, Idriss H, Keanne M A. Gold particle size effects in the gas-phase hydrogenation of m-dinitrobenzene over Au/TiO_2. Journal of Catalysis, 2009, 268(2): 223–234
12. Nguyen L Q, Salim C, Hinode H. Performance of nano-sized Au/TiO_2 for selective catalytic reduction of NO*x* by propene. Applied Catalysis A, General, 2008, 347(1): 94–99
13. Nguyen L Q, Salim C, Hinode H. Promotive effect of MO*x* (M = Ce, Mn) mechanically mixed with Au/TiO_2 on the catalytic activity for nitrogen monoxide reduction by propene. Topics in Catalysis, 2009, 52(6-7): 779–783
14. Chang Y C, Chen D H. Catalytic reduction of 4-nitrophenol by magnetically recoverable Au nanocatalyst. Journal of Hazardous Materials, 2009, 165(1-3): 664–669
15. Damato T C, Oliveira C S, Ando R A, Camargo P H C. A facile approach to TiO_2 colloidal spheres decorated with Au nanoparticles displaying well-defined sizes and uniform dispersion. Langmuir, 2013, 29(5): 1642–1649
16. Yazid H, Adnan R, Farrukh M A. Gold nanoparticles supported on titania for the reduction of *p*-nitrophenol. Indian Journal of Chemistry, 2013, 52A(2): 184–191
17. Hyuntae K, Miran K, Park K H. Effective immobilization of gold nanoparticles on core-shell thiol-functionalized GO coated TiO_2 and their catalytic application in the reduction of 4-nitrophenol. Applied Catalysis A, General, 2015, 502(1): 239–245
18. Kip C, Maras B, Evirgen O, Tuncel A. A new type of monodisperse porous, hydrophilic microspheres with reactive chloroalkyl functionality: Synthesis and derivatization properties. Colloid & Polymer Science, 2013, 292(1): 219–228
19. Günal G, Kip Ç, Öğüt S E, İlhan H, Kibar G, Tuncel A. Comparative DNA isolation behaviours of silica and polymer based sorbents in batch fashion: Monodisperse silica microspheres with bimodal pore size distribution as a new sorbent for DNA isolation. Artificial Cells, Nanomedicine, and Biotechnology, 2018, 46(1): 178–184
20. Hamaloğlu K Ö, Sağ E, Tuncel A. Bare, gold and silver nanoparticle decorated, monodisperse-porous titania microbeads for photocatalytic dye degradation in a newly constructed microfluidic, photocatalytic packed-bed reactor. Journal of Photochemistry and Photobiology A Chemistry, 2017, 332(1): 60–65
21. Camli T, Tuncel M, Senel S, Tuncel A. Functional, uniform, and macroporous latex particles: Preparation, electron microscopic characterization, and nonspecific protein adsorption properties. Journal of Applied Polymer Science, 2002, 84(2): 414–429
22. Tuncel A. Electron microscopic observation of uniform macroporous particles. II. Effect of DVB concentration. Journal of Applied Polymer Science, 1999, 71(14): 2291–2302
23. Ma Z, Guan Y, Liu H. Synthesis and characterization of micron-sized monodisperse superparamagnetic polymer particles with amino groups. Journal of Polymer Science Part A, 2005, 43(15): 3433–3439
24. Hamaloğlu K Ö, Sağ E, Tuncel A. Magnetic, monodisperse titania microspheres with bimodal pore size distribution by a new sol-gel templating method and their photocatalytic activity. Journal of Porous Materials, 2018,
25. Salimi K, Usta D D, Celikbicak O, Pinar A, Salih B, Tuncel A. Ti (IV) carrying polydopamine-coated, monodisperse-porous SiO_2 microspheres with stable magnetic properties for highly selective enrichment of phosphopeptides. Colloids and Surfaces. B, Biointerfaces, 2017, 153(1): 280–290
26. Jiao J, Wei Y, Zhao Y, Zhao Z, Duan A, Liu J, Pang Y, Li J, Jiang G, Wang Y. AuPd/3DOM-TiO_2 catalysts for photocatalytic reduction

of CO_2: High efficient separation of photogenerated charge carriers. Applied Catalysis B: Environmental, 2017, 209(1): 228–239

27. Wei Y, Wu X, Zhao Y, Wang L, Zhao Z, Huang X, Liu J, Li J. Efficient photocatalysts of TiO_2 nanocrystals-supported PtRu alloy nanoparticles for CO_2 reduction with H_2O: Synergistic effect of Pt-Ru. Applied Catalysis B: Environmental, 2018, 236(1): 445–457
28. Wei Y, Jiao J, Zhao Z, Liu J, Li J, Jiang G, Wang Y, Duan A. Fabrication of inverse opal TiO_2-supported Au@CdS core-shell nanoparticles for efficient photocatalytic CO_2 conversion. Applied Catalysis B: Environmental, 2015, 179(1): 422–432
29. Zhou Y, Zhu Y, Yang X, Huang J, Chen W, Lv X, Lia C, Li C. Au decorated Fe_3O_4@TiO_2 magnetic composites with visible light-assisted enhanced catalytic reduction of 4-nitrophenol. RSC Advances, 2015, 5(62): 50454–50461
30. Zheng J, Wu Y, Zhang Q, Li Y, Wang C, Zhou Y. Direct liquid phase deposition fabrication of waxberry-like magnetic Fe_3O_4@-TiO_2 core-shell microspheres. Materials Chemistry and Physics, 2016, 181(1): 391–396
31. Zhao Y, Wei Y, Wu X, Zheng H, Zhao Z, Liu J, Lia J. Graphene-wrapped Pt/TiO_2 photocatalysts with enhanced photogenerated charges separation and reactant adsorption for high selective photoreduction of CO_2 to CH_4. Applied Catalysis B: Environmental, 2018, 226(1): 360–372
32. Majumder S, Dey S, Bagani K, Dey S K, Banerjee S, Kumar S. A comparative study on the structural, optical and magnetic properties of Fe_3O_4 and Fe_3O_4@SiO_2 core-shell microspheres along with an assessment of their potentiality as electrochemical double layer capacitors. Dalton Transactions (Cambridge, England), 2015, 44(1): 7190–7202
33. Tahir K, Nazir S, Ahmad A, Li B, Shah S A A, Khan A U, Khan G M, Khan Q U, Khan Z U H, Khan F U. Biodirected synthesis of palladium nanoparticles using *Phoenix dactylifera* leaves extract and their size dependent biomedical and catalytic applications. RSC Advances, 2016, 6(89): 85903–85916
34. Dawson A, Kamat P V. Semiconductor-metal nanocomposites. Photoinduced fusion and photocatalysis of gold-capped TiO_2 (TiO_2/gold) nanoparticles. Journal of Physical Chemistry B, 2001, 105(5): 960–966
35. Kamat P V. Photophysical, photochemical and photo-catalytic aspects of metal nanoparticles. Journal of Physical Chemistry B, 2002, 106(32): 7729–7744
36. Pandikumar A, Murugesan S, Ramaraj R. Functionalized silicate sol-gel-supported TiO_2-Au core-shell nanomaterials and their photoelectrocatalytic activity. ACS Applied Materials & Interfaces, 2010, 2(7): 1912–1917
37. Wang Q, Li Y, Liu B, Dong Q, Xu G, Zhang L, Zhang J. Novel recyclable dual-heterostructured Fe_3O_4@CeO_2/M (M 1/4 Pt, Pd and Pt-Pd) catalysts: Synergetic and redox effects for superior catalytic performance. Journal of Materials Chemistry. A, Materials for Energy and Sustainability, 2015, 3(1): 139–147
38. Zhang Q, Jin X, Xu Z, Zhang J, Rendón U F, Razzari L, Chaker M, Ma D. Plasmonic Au-loaded hierarchical hollow porous TiO_2 spheres: Synergistic catalysts for nitroaromatic reduction. Journal of Physical Chemistry Letters, 2018, 9(1): 5317–5326
39. Linic S, Christopher P, Ingram D B. Plasmonic-metal nanostructures for efficient conversion of solar to chemical energy. Nature Materials, 2011, 10(12): 911–921
40. Bian Z F, Tachikawa T, Zhang P, Fujitsuka M, Majima T. Au/TiO_2 superstructure-based plasmonic photocatalysts exhibiting efficient charge separation and unprecedented activity. Journal of the American Chemical Society, 2014, 136(1): 458–465
41. Knight M W, Sobhani H, Nordlander P, Halas N J. Photodetection with active optical antennas. Science, 2011, 332(1): 702–704
42. Priebe J B, Karnahl M, Junge H, Beller M, Hollmann D, Bruckner A. Water reduction with visible light: Synergy between optical transitions and electron transfer in Au-TiO_2 catalysts visualized by in situ EPR spectroscopy. Angewandte Chemie International Edition, 2013, 52(1): 11420–11424
43. Zheng B Y, Zhao H Q, Manjavacas A, McClain M, Nordlander P, Halas N J. Distinguishing between plasmon-induced and photo-excited carriers in a device geometry. Nature Communications, 2015, 7797(6): 1–7
44. Mu B, Wang W, Zhang J, Wang A. Superparamagnetic sandwich structured silver/halloysite nanotubes/Fe_3O_4 nanocomposites for 4-nitrophenol reduction. RSC Advances, 2014, 4(1): 39439–39445
45. Jana S, Ghosh S K, Nath S, Pande S, Praharaj S, Panigrahi S, Basu S, Endo T, Pal T. Synthesis of silver nanoshell-coated cationic polystyrene beads: A solid phase catalyst for the reduction of 4-nitrophenol. Applied Catalysis A, 2006, 313(1): 41–48
46. Veerakumar P, Velayudham M, Lub K L, Rajagopal S. Polyelectrolyte encapsulated gold nanoparticles as efficient active catalyst for reduction of nitro compounds by kinetic method. Applied Catalysis A, 2012, 439-440(1): 197–205
47. Sarkar S, Guria A K, Pradhan N. Influence of doping on semiconductor nanocrystals mediated charge transfer and photo-catalytic organic reaction. Chemical Communications, 2013, 49(1): 6018–6020